J. Fluid Mech. (1980), *vol.* 100, *part.* 3, *pp.* 513–544
Printed in Great Britain

An experimental study of oscillatory pipe flow at transitional Reynolds numbers

By B. R. RAMAPRIAN AND SHUEN-WEI TU

Iowa Institute of Hydraulic Research,
The University of Iowa, Iowa 52242

(Received 15 May 1979 and in revised form 27 November 1979)

Fully developed oil flow in a smooth circular pipe at a mean Reynolds number of about 2100 was subjected to a nominally sinusoidal flow modulation at frequencies ranging from 0·05–1·75 Hz. It was observed that flow oscillation increased the critical Reynolds number and, under certain conditions, even brought about laminarization of the flow, which would be intermittently turbulent at the mean Reynolds number under quasi-steady (infinitely small oscillation frequency) conditions. The occurrence and extent of laminarization was, however, found to depend on factors such as the intermittency of turbulent puffs in the mean quasi-steady flow, frequency of oscillation, etc. Two series of experiments were performed. In one series, the oscillatory flow was almost completely laminarized. In the other series, the oscillatory flow was fully turbulent. In both the cases, instantaneous velocities in the flow were measured using laser–Doppler anemometry (LDA). The instantaneous velocity was decomposed into time-mean, periodic and random components employing ensemble-averaging techniques. The experiments indicated that the laminarized oscillatory flow behaves very similarly to laminar oscillatory flow at either end of the Strouhal-number range studied. The oscillatory turbulent flow was found to depend on both the Strouhal number and the ratio of the oscillation frequency (f) to some characteristic frequency (f_t) of turbulence in the flow. The design of the present experimental facility made it possible to study the flow at $f/f_t \approx 1$ ('high' oscillation frequency), a condition that could not be attained in most previous investigations. Another unique feature of the present experiment was that the viscous sublayer and Stokes layer were both large enough (several millimetres in thickness) to allow detailed measurements to be made in these regions. It was found, that at this high frequency of oscillation, the Reynolds stresses generally remained frozen at an average state during the entire oscillation cycle. The turbulent structure showed significant departures from equilibrium at all times during the oscillation cycle. As a result, there was a net change in the time-mean velocity profile near the wall and a net increase in the time-mean wall shear stress and power loss due to friction. The observation that unsteadiness can indeed affect the mean flow behaviour in a significant way is new and contradicts the view presently held by many researchers (based on their studies at relatively low oscillation frequencies, i.e. $f/f_t \ll 1$). The data also indicated that the direct interaction between oscillation and the turbulent structure was essentially confined to the Stokes layer. The study suggests that (again contrary to the existing belief) quasi-steady turbulence models may not be adequate to describe unsteady flows when the time scale of unsteadiness is comparable to that of dominant turbulent eddies.

0022-1120/80/4544-2070 $02.00

1. Introduction

The study of unsteady shear flows is relevant to many areas of application such as aerodynamics, ship hydrodynamics, biofluid mechanics and wind engineering. Much of the study reported in the literature on unsteady flows, however, concerns laminar flows. Exact solutions are available for relatively simple unsteady laminar flow situations in the classical literature (see Rosenhead 1963). Laminar flows in pipes due to periodic pressure gradients have been studied by Richardson & Tyler (1929), and Uchida (1956) and others. The situation with regard to unsteady transitional and turbulent flows is less satisfactory, however. While there have been some attempts to analyse the problem of stability in periodic flows (e.g. von Kerczek & Davis 1974, 1976; Hino & Sawamoto 1975; Hino, Sawamoto & Takasu 1976), much remains to be studied in this area. Of the laboratory experiments on periodic pipe flow that have been reported in the literature, most pertain to high-Reynolds-number turbulent flows. The earliest of such experiments were reported by Schulz-Grunow (1940). More recent experiments in this category are those performed by Hirose & Oka (1969), Lu *et al.* (1973) and Acharya & Reynolds (1975). In all these experiments fully developed turbulent pipe flow was perturbed by imposing a periodic modulation in discharge at a prescribed frequency. Of these, the work of Acharya & Reynolds involved the most detailed measurements such as Reynolds shear stress, though the amplitude of flow modulation in their experiments was less than 5 per cent of the mean. These experiments suggested that even at that amplitude, the structure of turbulence can be significantly affected in the Stokes layer near the wall. Their measurements in this layer were very limited because of the thinness of the layer. Lu *et al.* experienced considerable difficulty in the use of hot-film anemometry as well as in analog data processing in their experiments on oscillatory flow of water in a circular pipe. Their measurements of mean and turbulent velocities did not lead to any significant conclusions.

One would intuitively expect that the effects of unsteadiness on the flow structure will be stronger on flows in the neighbourhood of transition than on flows at very large Reynolds numbers. This is because transition process can be sensitive to the strong acceleration/deceleration in the unsteady flow. The experience with steady flows subjected to spatial pressure gradients has confirmed that the pressure gradients have a significant effect on the critical Reynolds number. Strong effects of periodic flow modulation on the flow characteristics at transitional Reynolds numbers have, indeed, been observed in the experiments of Sarpkaya (1966) and in the more recent studies of Gerrard (1971) and Hino & Sawamoto (1975). From a study of the growth of disturbances in sinusoidally modulated pipe flow in the mean flow Reynolds-number range of 2000–5000, Sarpkaya concluded that flow pulsation increases the critical Reynolds number. Gerrard's experiments related to periodic pipe flow at a mean Reynolds number of 3700 while the experiments of Hino & Sawamoto pertained to purely oscillatory pipe flow (i.e., at a mean Reynolds number of zero). These latter two studies were mainly qualitative but they indicated that, in general, turbulence is inhibited during the acceleration part of the modulation cycle and enhanced during the retardation part. In fact, the flow, under certain circumstances, appeared to remain laminar during the acceleration part of the cycle. Indications of inhibition of turbulence or delayed transition have also been observed in some of the *in-vivo* studies of pulsatile

blood flow in the aorta of mammals (e.g. Falsetti *et al.* 1972; Kiser *et al.* 1976). However, the instrumentation and data reduction techniques used in the blood-flow studies, as well as in the other laboratory studies mentioned above, were not sufficiently sophisticated to yield detailed quantitative information on the flow structure.

There is one class of unsteady turbulent flows, however, that has been studied in fair detail using moderate to highly sophisticated data reduction techniques. This is the unsteady turbulent boundary layer in a periodic free stream. Most of these studies (Karlsson 1959; Houdeville, Desopper & Cousteix 1976; Cousteix, Desopper & Houdeville 1977; Patel 1977) pertain to zero pressure-gradient boundary layers though some experiments on adverse pressure gradient flows have been reported recently (Kenison 1977; Houdeville & Cousteix 1978). The experiments on the zero pressure-gradient boundary layers have, generally, led to the conclusion that flow modulation has no effect on the average behaviour of the flow and that the turbulent structure can still be described by quasi-steady turbulence models. A careful study of these investigations, however, reveals that in all these experiments, the frequency of flow modulation was small compared with the characteristic frequency of turbulence in the boundary layer. One can expect to find a significant effect of flow modulation on the average flow structure only when the modulation frequency is comparable to the characteristic turbulent frequency in the flow. The very recent report of Houdeville & Cousteix (1978) on the unsteady boundary layer in the neighbourhood of separation (where this condition is satisfied) does seem to indicate strong effects of flow modulation on the flow structure. Hence, the behaviour of an unsteady turbulent flow is not only determined by the Strouhal number (ratio of the time scale of mean flow to the time scale of unsteadiness), but also by the ratio of the time scale of unsteadiness to the characteristic time scale of turbulence. Further, since most of the interaction between the impressed oscillation and the turbulence structure is likely to occur within the Stokes layer, it is necessary to design the experiment carefully so as to get a thick enough Stokes layer and yet keep the modulation frequency at a value comparable to the characteristic turbulent frequency.

The present study was directed towards obtaining experimental data on fully developed oscillatory pipe flow at transitional Reynolds numbers. The nature of the periodic flow was found to depend strongly on the nature of the steady flow at the mean Reynolds number. It was found that if the steady mean flow was fully turbulent (with an intermittency of unity), the flow would remain fully turbulent when the Reynolds number was modulated at a frequency large enough to approach the characteristic turbulent frequency. On the other hand, if the steady mean flow was not turbulent but contained turbulent puffs at a low intermittency, the flow would tend to laminarize on periodic oscillation. Both these flow situations were studied in detail using laser–Doppler anemometry (LDA) together with a digital phase-averaging technique. Important features of the present experiments, particularly with regard to the turbulent unsteady flow, are (i) the oscillation frequency was high enough to be comparable to the characteristic turbulence frequency in the flow with the amplitude of flow modulation being large enough to be significant, and (ii) the viscous sublayer (2 mm) and Stokes sublayer (6 mm) were thick enough to permit detailed measurements in a region where the interaction of flow oscillation and turbulence have been found to be very strong. These features distinguish the present experiments from other basic unsteady turbulent flow experiments reported so far in the literature.

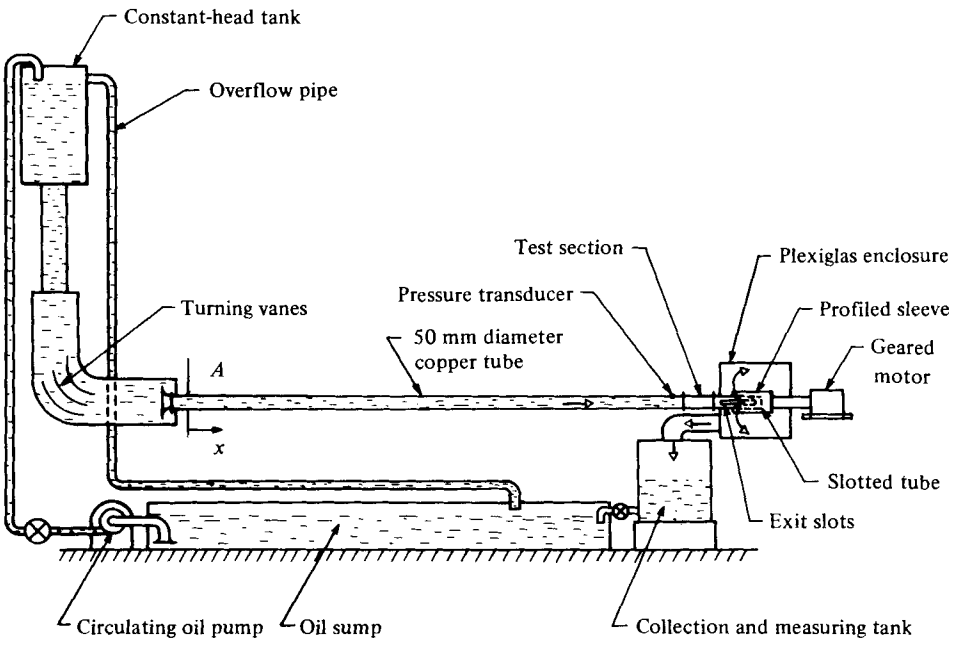

FIGURE 1. Schematic layout of the experiment apparatus.

2. Experimental details

2.1. *The apparatus*

A test facility for producing periodic pipe flow at transitional Reynolds number was built for the present study. The facility used 'Eureka' oil – a clear fluid of kinematic viscosity, $\nu = 1{\cdot}384 \times 10^{-5}$ m^2 s^{-1} at 26 °C. A schematic layout of the apparatus is shown in figure 1. A brief description of the apparatus is given below. A more detailed description can be found either in Tu (1978) or Ramaprian & Tu (1979).

Oil from the constant head tank entered the copper tube of 50 mm internal diameter (D) and 8·8 m length (L) through an inlet pipe and a bell shaped contraction. Static pressure taps of 1 mm diameter were provided at regular intervals along the tube. The test section where velocity measurements were made was a 50 mm internal diameter, 0·3 m long Plexiglas tube located at the end of the copper tube. The test section was followed by another copper tube 0·3 m long closed at the downstream end. The oil came out through a pair of longitudinal rectangular slots of nominal size 50 × 3 mm milled on the surface of this tube at two diametrically opposite locations. The exit area was varied by a profiled brass sleeve rotating over the slotted tube. The sleeve profile consisted of a sine wave of two cycles. The sleeve was rotated by a geared d.c. motor whose speed was electronically regulated to remain within 1 per cent of any preset speed in the range 1·2–55 r.p.m. It is seen that, with this design, the exit area variation would be a sinusoidal function of time with the variation going through 2 cycles during each revolution of the sleeve. A magnetic pickup was used to produce a pulse *once* during each *revolution* of the sleeve. This pulse was synchronized with the instant of maximum slot opening and was used as the reference signal during data acquisition and processing. The mean exit area could be adjusted

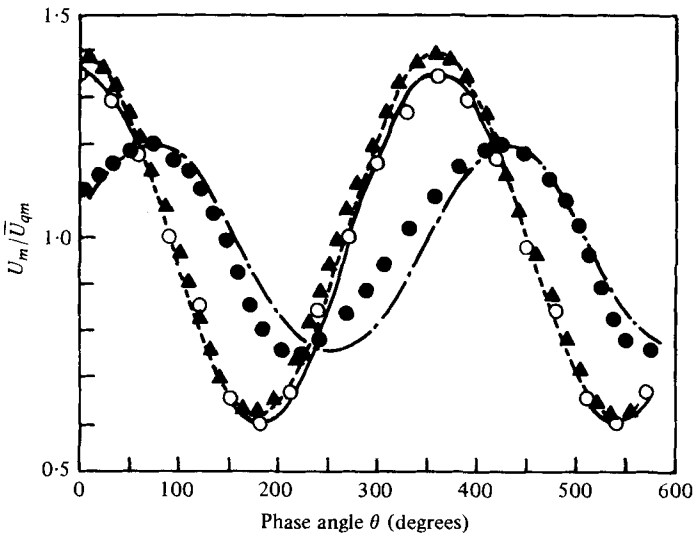

FIGURE 2. Variation of the cross sectional average velocity during a cycle: ○, quasi-steady; ▲, oscillatory flow at 0·057 Hz (run 24); ●, oscillatory flow at 1·75 Hz (run 13). Lines denote exact sine waves with corresponding amplitudes: ——, quasi-steady; – – –, 0·057 Hz; – · –, 1·75 Hz.

within limits by changing the axial location of the sleeve relative to the slots. In the present study, this location was chosen (after several trial runs) such that the time-mean flow Reynolds number $\overline{Re}$ (defined as $\bar{U}_m D/\nu$) was about 2100 (corresponding to a time-mean cross-sectional average velocity $\bar{U}_m$ of about 0·55 m s^{-1}). The sleeve profile was designed for an estimated discharge modulation amplitude of 0·35 × mean discharge. Later tests showed that the actual discharge modulation under quasi-steady conditions (i.e., at extremely low modulation frequencies) was, in fact, quite close to this value. With the present design, the flow was found to be fully laminar at the minimum slot opening and fully turbulent at the maximum slot opening under steady or quasi-steady condition. Further, it was found (as expected) that a nearly sinusoidal discharge modulation could be obtained under quasi-steady conditions. This is, seen from figure 2, which shows the variation of the quasi-steady cross sectional average velocity, U_{qm} (proportional to the quasi-steady discharge) with the phase angle θ, (measured with reference to the instant of maximum slot opening) during the modulation cycle. The data shown in this figure were obtained by measuring the steady flow discharge (using a measuring tank) at various *fixed* angular positions (θ) of the sleeve. The data are normalized with respect to their time average value $\bar{U}_{qm}$ and, are compared with an exact sine curve having the same maximum and minimum values.

When the discharge is modulated at a finite frequency by rotating the sleeve, the discharge variation during the cycle will differ from the quasi-steady distribution. This is mainly due to the effect of fluid inertia. As a consequence, the amplitude of modulation will decrease, the modulation will be distorted from the sinusoidal shape and the pressure at any point in the system will oscillate with a significant amplitude. These effects will increase with the frequency of flow oscillation. Further, at the higher oscillation frequencies, the discharge and pressure variations will, in general, be out

of phase with each other and with the exit area variation. The effect on the discharge, in particular, was, indeed found to follow the above trend. This can be seen typically from figure 2 where the variation of cross-sectional average velocity, U_m in unsteady flow is plotted for two oscillation frequencies. The distortion from the sine wave is seen to be negligible at the lower frequency of 0·057 Hz but perceptible at the higher frequency of 1·75 Hz. It was, however, decided to ignore this distortion in the present study as it was not considered to be a critical factor for the purpose of the present investigation.

2.2. *Instrumentation and data acquisition*

The instantaneous velocity in the flow was measured using the LDA. The LDA system consisted of a 5 mW He–Ne laser illuminating a TSI (Thermo-Systems Inc.) optics, a photo-multiplier and a frequency tracker. In addition, the system had a frequency-shift feature which enabled very low velocities and flow reversals to be studied. The LDA system could be traversed along a horizontal diameter of the test section, for obtaining the velocity profile across the test section. A detailed description of the LDA system and the traverse is given in Ramaprian & Tu (1979). The LDA was used in the dual beam mode. The measurement configuration used in the present experiments resulted in a measuring cross section about $1 \times 0{\cdot}5$ mm, with the longer dimension located (unavoidably) along the radius. However, this poor spatial resolution was not very serious, in view of the fact that the viscous-sublayer thickness in the flow was about 2 mm.

The LDA output is the instantaneous axial velocity, U as a function of time and can be decomposed as

$$U(r,\theta,t) = \overline{U}(r) + U_p(r,\theta) + u(r,\theta,t) \tag{1}$$

$$= \langle U(r,\theta)\rangle + u(r,\theta,t), \tag{2}$$

where $\overline{U}$ is the time-mean velocity at radius r and time t, u is the turbulent (random) velocity and $\langle U\rangle$ is the deterministic velocity or the sum of $\overline{U}$ and the periodic component U_p. In an unsteady flow, the deterministic velocity can be obtained by a process of ensemble averaging. In the particular case when the unsteady flow is periodic, ensemble averaging is equivalent to phase averaging; i.e., averaging over the values obtained at identical values of r and θ in a large number of oscillation cycles.

In the present experiments the data-acquisition system was programmed to sample the LDA output at the end of each prescribed sampling interval (ΔT), starting from the instant when the synchronizing reference signal from the magnetic pick up was received. The interval, ΔT was chosen to be approximately 1/100 the period of one sleeve revolution (and hence about 1/50 of the period of a cycle). A total of 100 sleeve revolutions (rather than oscillation cycles) were used for phase averaging at the higher frequency of 1·75 Hz studied. At the lower frequency of 0·057 Hz, 25 revolutions were used (since there was no turbulence to be measured in this case). The sampled data were digitized and processed to obtain the velocities $\overline{U}$, $\langle U\rangle$, $\langle u^2\rangle$, etc. In each case, the experiments were repeated thrice and the results averaged over the three experiments. If the results in consecutive experiments differed significantly from one another, the experiments were repeated till three consecutive experiments gave nearly the same results. (Such repetitions were, however, rarely necessary.) The value of $\overline{U}$ varied insignificantly among consecutive experiments, while the scatter in $\langle U\rangle$ was

generally within 1 per cent and the scatter in u_p' (defined as $\langle u^2 \rangle^{\frac{1}{2}}$) within 5 per cent. The data acquisition program was designed to detect any 'drop-out' of the signal from the LDA and reject all the samples taken during that entire sleeve revolution. Data acquisition would then proceed until the required number of valid revolutions were sampled. However, with the use of frequency-shift feature of the LDA, there was virtually no problem of signal drop out and this feature of the program was rarely made use of. More details on data acquisition are given in Ramaprian & Tu (1979).

The above scheme was also used for processing unsteady laminar flows, the value of u_p' in this case being used as a measure of the noise in the optics and electronics. It was found that u_p' ranged from 2–5 parts in 1000 in these cases, indicating the acceptability of the experimental procedure.

2.3. *Experimental details*

As already mentioned, two series of experiments were carried out. In both the series, the steady flow had a Reynolds number of about 2900 at maximum slot opening ($\theta = 0°$). The mean steady-flow Reynolds number was about 2100 and this occurred at $\theta \cong 90°$. However, in the first series, the steady flow at $\theta = 90°$ was found to be fully turbulent at all times. In fact, the intermittency of turbulence remained at unity for $\theta \lesssim 100°$. When this flow was oscillated at the highest possible frequency of 1·75 Hz, the flow remained fully turbulent. Instantaneous velocity measurements were obtained across the pipe for this situation (run 13). A rough estimate of the turbulent burst frequency in this flow using the criterion of Rao, Narasimha & Badri Narayanan (1971) indicates a value of about 2 Hz. Thus the oscillation frequency can be expected to interact significantly with the turbulent structure in this flow. In the second series of experiments, while the steady flow at the maximum and minimum slot opening behaved exactly as in the first series, the mean flow at $\theta = 90°$ exhibited an intermittent turbulent structure. The structure strongly resembled the puff-type transitional structure studied by Wygnanski & Champagne (1973). In fact, the steady flow became fully turbulent only at values of $\theta \lesssim 60°$. When this flow was oscillated (at whatever frequency) it was found to laminarize with the intermittency of puffs dropping almost to zero. This is clearly seen from figure 3 where a photograph of the storage oscilloscope traces corresponding to the centre-line velocity signals obtained from the LDA under three different conditions are shown superimposed on one another. These are: (i) steady flow at $\theta = 0°$, $Re = 2872$ (fully turbulent); (ii) steady flow at $\theta = 180°$, $Re = 1278$ (fully laminar); and (iii) oscillatory flows at 0·057 Hz between the above two Reynolds numbers (laminarized). The peak velocity in the oscillatory flow is different from the velocity in steady turbulent flow because the unsteady flow is laminar and hence has a different velocity distribution. Velocity measurements were made in this laminarized unsteady flow at oscillation frequencies of 1·75 Hz (run 23) and 0·057 Hz (run 24). These frequencies correspond to Strouhal numbers S (defined as $2\pi f D/\overline{U}_m$) of 1·0 and 0·032 respectively.

In both the series, measurements of velocity distribution in the pipe were made for the steady flows at $\theta = 0$ and $\theta = 180°$. In addition, steady flow axial pressure drop data were obtained for several (fixed) angular positions, θ of the sleeve. These measurements (reported in detail in Ramaprian & Tu 1979) indicated full development of the mean flow beyond $x/D = 100$. They also confirmed that the apparatus was functioning normally and that the flow was transitional. Further, these steady flow

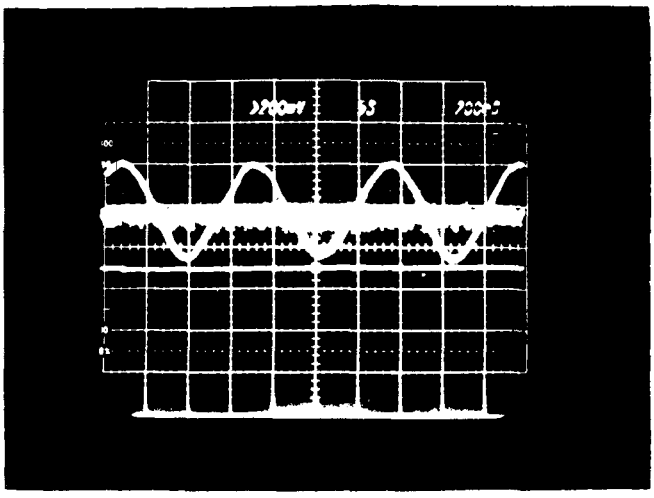

FIGURE 3. Oscilloscope traces of velocity signals from LDA ($r = 0$). The smooth horizontal trace corresponds to steady laminar flow ($\theta = 180°$); the hashed horizontal trace corresponds to steady turbulent flow ($\theta = 0°$); the smooth sinusoidal trace corresponds to laminarized oscillatory flow.

experiments can be considered to approximate closely to quasi-steady experiments. They are used as a reference in the study of the unsteady flow behaviour. The use of these data instead of steady flow data from other sources is both necessary and desirable in view of the very low Reynolds numbers and transitional nature of the flow.

3. Results and discussion

3.1. *Steady-flow measurements*

3.1.1. *Velocity distribution.* The results of velocity measurement at $\theta = 180°$ (minimum slot opening) and $\theta = 0°$ (maximum slot opening) are shown in figure 4. In each case, data obtained in both the series of experiments are shown even though fewer points are shown for series 2. This is considered adequate in view of the excellent repeatability observed between the two series of steady flow experiments. In the case of laminar flow ($\theta = 180°$), the data are seen to agree well with the theoretical parabolic profile. It is seen from the figure that the mean velocity profiles in turbulent flow obtained from the two series of experiments also indicate agreement with each other. The agreement between the two sets of data obtained with a gap of several months in between establishes the accuracy of the measurement procedure. It also confirms that the behaviour of the quasi-steady flow at both the maximum and minimum end of the oscillation cycle did not change even though the transitional character at intermediate Reynolds numbers had changed.

The velocity profile for the turbulent flow at $\theta = 0°$ is shown in figure 5 in the usual wall-layer co-ordinate $U^+ (= \overline{U}/u_*)$ *vs.* $Y^+ [= (1 - 2r/D)\, Du_*/2\nu]$, u_* being the shear velocity $(\tau_w/\rho)^{\frac{1}{2}}$ where τ_w is the wall shear stress. The value of u_* was obtained from the quasi-steady pressure drop and discharge data for $\theta = 0°$ using the relation,

$$\lambda_q = \frac{1}{8}\frac{u_*^2}{U_{qm}^2}. \tag{3}$$

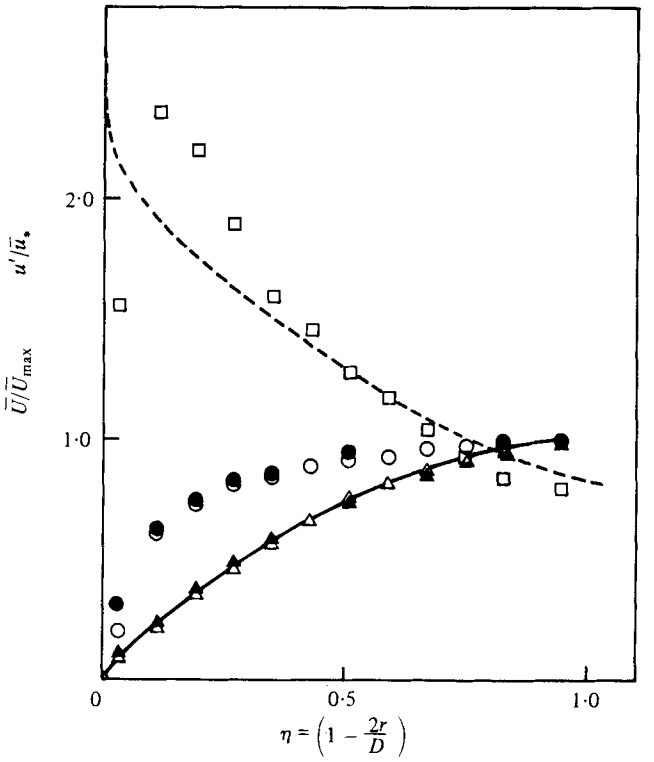

FIGURE 4. Distributions of mean and turbulent velocities in steady flow: △, run 11; ▲, run 21. Laminar flow at $\theta = 180°$ ($Re = 1278$): ○, run 12; ●, run 22. Turbulent flow at $\theta = 0°$ ($Re = 2870$): ——, theoretical parabolic profile for laminar flow. Turbulent intensity: □, run 12; – – –, data from Laufer (1954) for $Re = 5 \times 10^5$.

The measured velocity distribution is compared with the universal law of the wall, namely, $U^+ = Y^+$ in the viscous sublayer and $U^+ = 5{\cdot}75 \log Y^+ + 5{\cdot}5$ in the fully turbulent region. The deviation of the experimental data from the universal log law is to be expected in view of the very low Reynolds number of the flow. On the other hand, the fact that the first data point near the wall falls on the linear $U^+ = Y^+$ curve indicates not only that this point is in the viscous sublayer but also that the value of u_* is accurate.

3.1.2. *Turbulence intensity distribution.* Figure 4 introduced earlier, also shows the distribution of the r.m.s. intensity, u' $\left(\text{defined as } \left(\frac{1}{2\pi}\int_0^{2\pi} \langle u^2 \rangle \, d\theta\right)^{\frac{1}{2}}\right)$ of the longitudinal turbulent velocity fluctuations in the steady turbulent flow at $\theta = 0$. The distribution is normalized using the velocity and length scales, u_* and $\frac{1}{2}D$ respectively. Consequently, the distribution can be expected to show Reynolds number dependence in the inner region. This is, in fact, the case as is seen from the comparison with the data of Laufer (1954) obtained at a Reynolds number of 5×10^5. The distribution in the region $0{\cdot}5 < \eta = (1 - 2r/D) < 1$ is seen to coincide reasonably well with Laufer's data while in the region $(1 - 2r/D) < 0{\cdot}5$, a strong Reynolds-number effect is observed. In fact, the large viscous region in the present case allows one to observe the gradual decrease

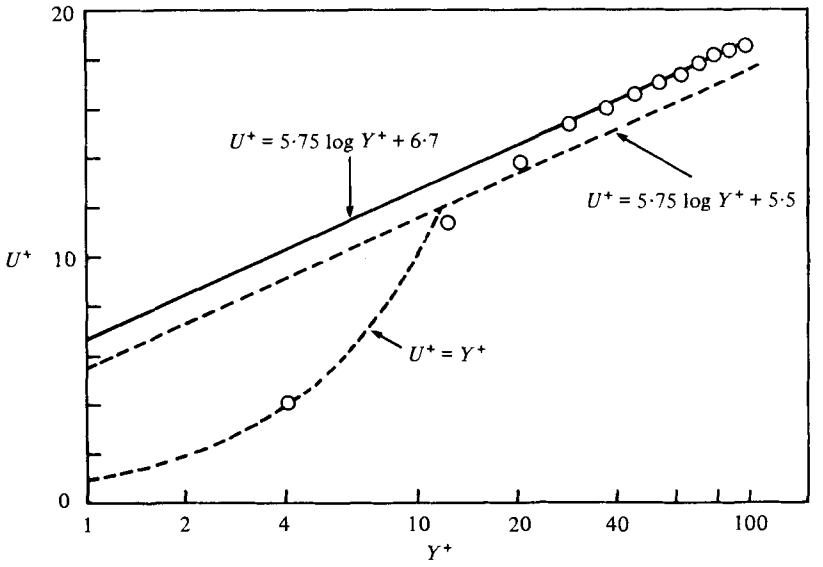

FIGURE 5. Velocity distribution in steady flow in wall-layer co-ordinates: $\theta = 0$ (maximum slot opening).

of u' from a maximum towards zero at the wall, a feature which is usually difficult to observe in higher-Reynolds-number laboratory flows. The purpose of presenting the steady-flow turbulence distribution in figure 4 is to provide a basis for the comparison with the unsteady turbulent-flow data. It is clear that it is very important to make comparisons in approximately the same Reynolds-number range in order to arrive at reliable conclusions.

3.2. *Unsteady flow measurements*

3.2.1. *Velocity distribution in unsteady flow.* Figure 6 shows the distribution of the time-averaged velocity $\overline{U}$ across the pipe in the three runs 13, 23 and 24. The velocities, in each case, are normalized with respect to the corresponding velocity at the pipe axis ($\overline{U}_{max}$). The distributions are compared with the quasi-steady velocity distributions corresponding to $\theta = 180°$ and $\theta = 0°$. It is seen from the figure that the unsteady flows in run 23 and 24 that appeared to be laminar were, indeed, very nearly laminar i.e., they exhibit nearly parabolic velocity distributions. In fully developed oscillatory laminar pipe flow of a Newtonian fluid, the time-mean velocity distribution should be identical to that of steady Poiseuille flow since the velocity field is determined from the linear equation

$$\frac{\partial U}{\partial t} = -\frac{1}{\rho}\frac{\partial P}{\partial x} + \nu\left[\frac{\partial^2 U}{\partial r^2} + \frac{1}{r}\frac{\partial U}{\partial r}\right]. \tag{4}$$

It is seen that, in the high frequency run 23, in which the intermittency of turbulent puffs was very small (as already mentioned), the time-mean unsteady flow behaves almost exactly like laminar flow. The deviation of the experimental data of run 24 from the parabolic profile has been caused by the flow becoming turbulent with a larger intermittency than in run 23. It is, however, important to observe from figure 6

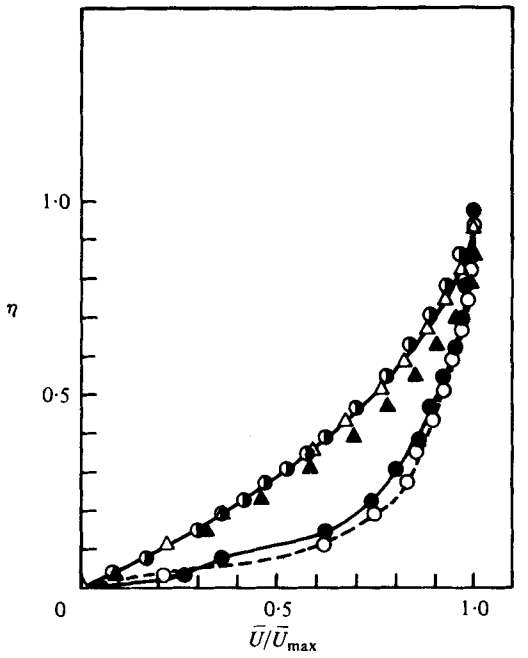

FIGURE 6. Distribution of the time-mean velocity across the pipe in unsteady flow. △, steady laminar flow (θ = 180°); —○—, steady turbulent flow (θ = 0°); —●—, unsteady turbulent flow at f = 1·75 Hz (run 13); ◑, unsteady laminarized flow at f = 1·75 Hz (run 23); ▲, unsteady laminarized flow at f = 0·057 Hz (run 24); ——, theoretical parabolic profile for laminar flow.

that the effect of flow oscillation on the time-mean velocity gradient and hence the wall shear stress, is negligible in both these runs.

When the oscillatory flow is turbulent, the total shear stress (τ) distribution in the pipe is given by the linear equation

$$\frac{\partial U}{\partial t} = -\frac{1}{\rho}\frac{\partial P}{\partial x} + \frac{1}{\rho r}\frac{\partial(\tau r)}{\partial r} \tag{5}$$

and hence the distribution of time-averaged shear stress, $\bar{\tau}$ should be linear as in steady turbulent flow. However, since $\bar{\tau}$ is now given by

$$\bar{\tau}/\rho = \nu\frac{\partial \bar{U}}{\partial r} - \overline{uv} \tag{6}$$

(where u and v are the turbulent velocity fluctuations in the x and r directions, respectively), the velocity field is not determined by a linear equation. The time-averaged velocity distribution, and hence the time averaged wall shear stress need not, therefore, be necessarily the same as in the steady flow at the mean Reynolds number. It is, in fact, seen from figure 6 that the time-mean velocity distribution in the unsteady turbulent flow of run 13 exhibits a point of inflexion near the wall and thus differs from the steady-state turbulence velocity profile. The time-mean velocity gradient at the wall is slightly larger than in the steady case resulting in a larger time-mean wall shear stress. This observation differs from those reported by previous investigators

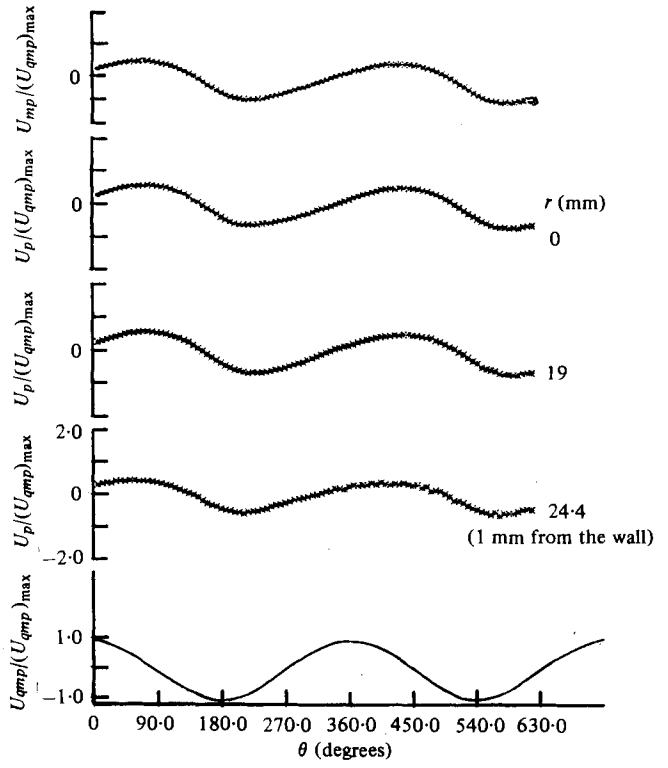

FIGURE 7. Variation of the periodic component of the velocity with phase angle. (*a*) Run 13; (*b*) run 23; (*c*) run 24.

of oscillatory turbulent boundary layers, who concluded that unsteadiness has no effect on the time-mean properties (or even the turbulent structure) of the flow. However, as already mentioned, a significant difference between the present experiment and the earlier experiments is that the oscillation frequency in the present case is comparable to the characteristic turbulent frequency.

Figure 7 presents the variation of the periodic component U_p of the velocity through the oscillation cycle at a few typical points across the pipe. The velocity is normalized with respect to the amplitude $(U_{qmp})_{max}$ of the quasi-steady cross sectional averaged periodic velocity. The variations are shown only for 700 degrees of oscillation cycle (slightly less than one full sleeve rotation), short record gaps being present (for reasons described in Ramaprian & Tu 1979) from 0–7·2° and 698·4–720°. Also for run 13, the data are shown only for 600 degrees of oscillation cycle, due to some difficulties encountered during data acquisition. These difficulties were subsequently removed before the second series of experiments were started. However, since data over only 360 degrees of oscillation cycle are sufficient for the purpose of analysis, the loss of redundant data is not serious. In each of the figures 7(*a*, *b*, *c*), the distributions of the unsteady cross sectional average periodic velocity, U_{mp} and quasi-steady cross sectional average periodic velocity, U_{qmp} (proportional to the effective modulation in exit area) are also shown for comparison. The latter curve is the same as the periodic part of the velocity distribution shown in figure 2. A comparison of the laminar flow data for

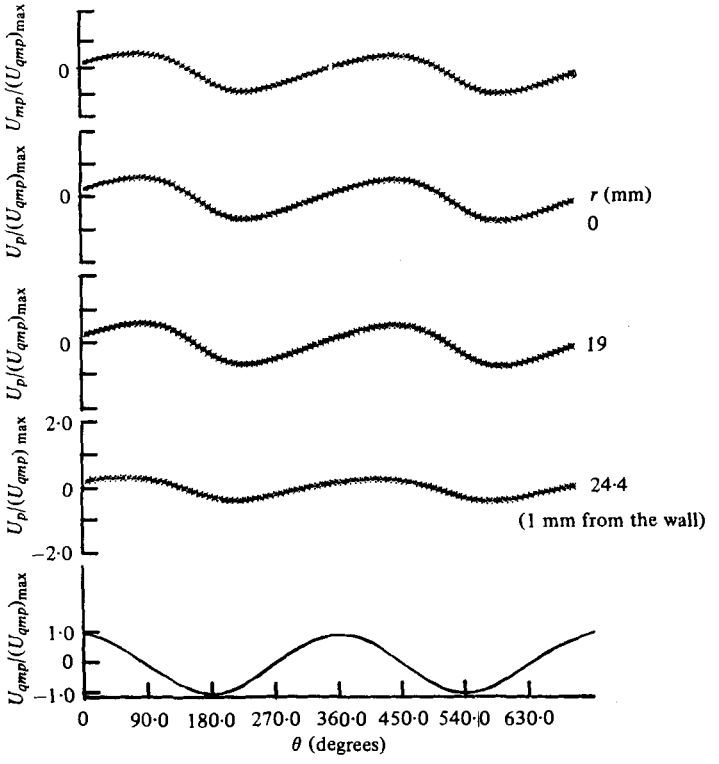

FIGURE 7 (*b*). For legend see facing page.

runs 23 and 24 shows that the phase-wise variations are strongly dependent on the oscillation frequency. The variations appear to be very nearly sinusoidal at the lower frequency while significant distortion in the wave shape can be observed at the higher oscillation frequency. The distortion at the higher frequency is, as mentioned earlier, due to nonlinear effects.

It is also clear from the figures 7 (*a*) and (*b*) that at the higher oscillation frequency, there is a significant phase shift between the velocity variation and the exit area opening. Most of this phase shift is brought about by the global dynamics of the system and is observable as the phase shift of unsteady cross sectional average flow. However, there is also a relative phase shift between the local velocity and the cross sectional average velocity. The flow in the wall region leads the cross sectional average flow while the flow in the core region lags behind the average flow. Unfortunately, owing to the uncertainty in phase angle measurement ($\pm 3{\cdot}5°$) and the distortion in the modulation profile, it is not possible to make a precise quantification of the phase differences nor is it possible to look for differences between the laminar and turbulent flow.

Figures 8 (*a*, *b*, *c*) shows cross plots of the distribution of the periodic velocity, U_p across the pipe for a few typical fixed phase angles in the oscillation cycle. It is seen that at the higher oscillation frequency, the variations in U_p are confined essentially to $\eta \lesssim 0{\cdot}25$ (i.e., the Stokes layer), the rest of the flow oscillating virtually as one solid mass at all times. At the lower frequency, U_p varies across the entire pipe at all

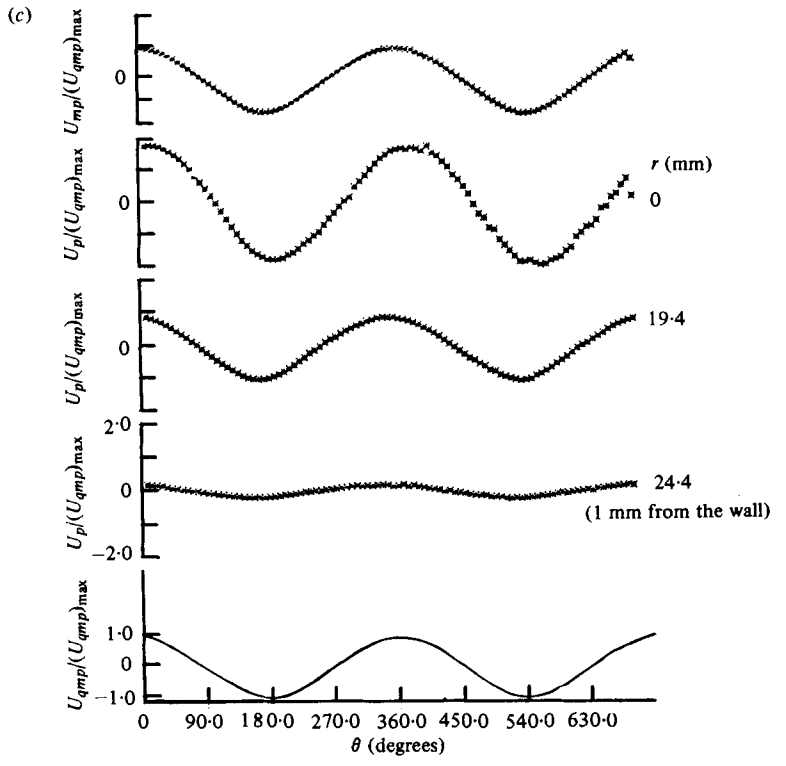

FIGURE 7(c). For legend see page 524.

times. The responses of turbulent and laminar flows appear to be qualitatively similar. It is seen that even at the higher frequency, the Stokes layer is about 6 mm thick.

Figure 9 shows the distribution of the 'amplitude', $(U_p)_{max}$ of the periodic velocity across the pipe for the three experiments. Since the velocity modulation is distorted from a sine wave especially at the higher frequency, it is not strictly appropriate to use the term 'amplitude' without making a formal harmonic analysis. However, in the present case, $(U_p)_{max}$ denotes one half of the peak to peak variation in the periodic velocity U_p. In the figure $(U_p)_{max}$ is normalized with respect to the amplitude $(U_{mp})_{max}$ of the cross sectional average periodic velocity. It is more clearly seen from this figure that at the higher frequency, the amplitude variations are confined to a small region ($\eta \lesssim 0{\cdot}25$) near the wall while at the lower frequency the variations extend over the entire pipe cross-section. The dominant effect of oscillation frequency is clearly seen from this figure. Also shown in this figure are the results computed from the exact solution of Uchida (1956) for fully developed laminar periodic flow in a pipe under the influence of a pressure gradient sinusoidally varying with time. The pressure gradient variation in the present experiments differed significantly from sinusoidal especially at the higher frequency. Yet, the experimental data for the laminar unsteady flows (runs 23 and 24) seem to agree reasonably well with the corresponding exact solutions. The somewhat larger discrepancy observed in the case of run 24 is possibly due to the intermittency effect mentioned earlier. It is interesting to note that the turbulent flow data (run 13) are not generally very different from the laminar flow data (run 23) at

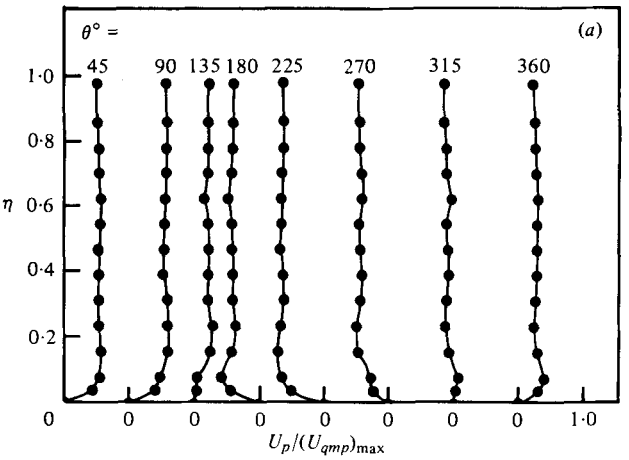

FIGURE 8. Distribution of the periodic component of the velocity across the pipe at fixed phase angle: (*a*) in oscillating turbulent flow, f = 1·75 Hz (run 13); (*b*) in oscillating laminar flow, f = 1·75 Hz (run 23); (*c*) in oscillating laminar flow, f = 0·057 Hz (run 24).

the same frequency. It is, however, seen that the turbulent flow data exhibit a somewhat larger overshoot in the Stokes layer.

3.2.2. *Effect of flow modulation on turbulence and transition.* The data obtained in the two series of present experiments provide some insight into the effects of impressed unsteadiness on the structure of turbulence and transition in pipe flow. For convenience, the two series of experiments will be discussed one by one.

(*a*) *Results of series* 1 *experiments*: (*turbulent unsteady flow*). The distribution of the r.m.s. turbulent intensity u', normalized with respect to $\overline{u}_*$† is shown in figure 10. Comparison with the steady flow data for $\theta = 0$ shows that in the oscillatory flow there is a slight decrease in the maximum turbulence intensity near the wall, while the turbulence intensity farther away from the wall is not affected. The near-wall region where the turbulent intensity is affected extends approximately over 25 per cent of the pipe radius and this region coincides with the Stokes layer where significant effects of flow oscillation are observed on the time-mean and periodic structures of the flow also. This result is in agreement with the conclusions of Acharya & Reynolds (1975) that the structure of turbulence is primarily affected within the Stokes layer. The distributions of the ensemble averaged turbulence intensity $u'_p(\theta)$ normalized with respect to the corresponding shear velocity $u_{*p}(\theta)$ are also shown in figure 10

† The shear velocity $u_{*p}(\theta)$ in unsteady flow was obtained from the ensemble-average velocity gradient at the wall. The velocity gradient at the wall was calculated from the measured $\langle U(\theta)\rangle$ at the first point near the wall assuming a linear velocity distribution in the viscous sublayer at all instants. This procedure was found to be generally satisfactory as verified from checks made in steady laminar and turbulent flow. In these cases, the wall shear stress obtained by this method compared well (within 3 %) with the value obtained from pressure drop measurements. From the ensemble-averaged value u_{*p}, the time-averaged value $\overline{u}_*$ was obtained from the relation

$$\overline{u}_*^2 = \frac{1}{2\pi}\int_0^{2\pi} u_{*p}^2\, d\theta.$$

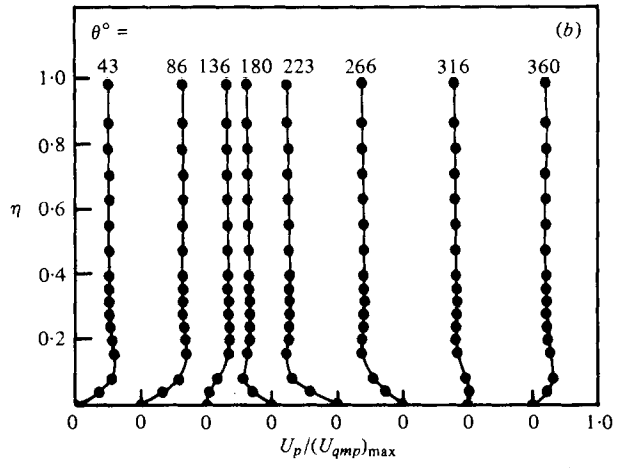

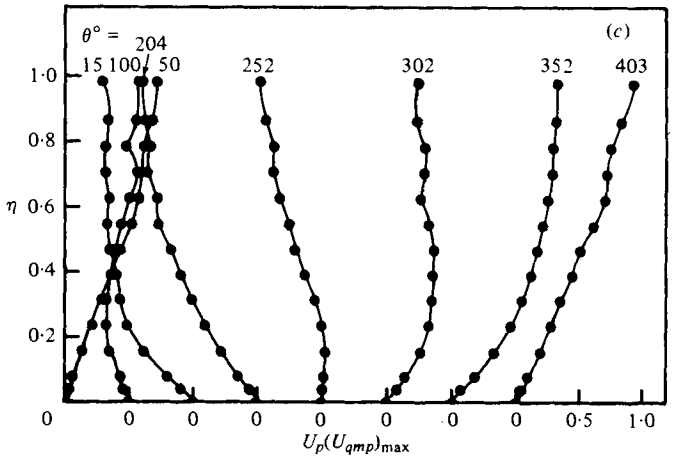

FIGURES 8(*b*, *c*). For legend see page 527.

for a few typical fixed angles of the oscillation cycle. Large variations in the distributions from one another and from the distribution of $u'/\overline{u}_*$ indicate that the turbulence structure is highly disturbed from equilibrium. The variations in the relative turbulent intensity (u'_p/u_{*p}) with time are shown in figure 11 for two typical locations across the pipe. These figures suggest that the flow was undergoing rapid structural distortion in time. Actually the wall shear stress (u_{*p}) could nearly follow the changes through the discharge cycle while the turbulent u fluctuations could not. This is seen clearly from figure 11 which also shows the variation of u_{*p} and the variation of u'_p (not normalized) at these two typical points in the pipe. It is seen that u_{*p} oscillates with a slight phase lead with respect the cross-sectional average periodic velocity U_{mp}, while u'_p remains practically constant throughout the oscillation cycle. Such a freezing of the turbulent normal stress can be expected to occur when the flow is subjected to rapid strain rates, i.e. when changes occur at time scales comparable to

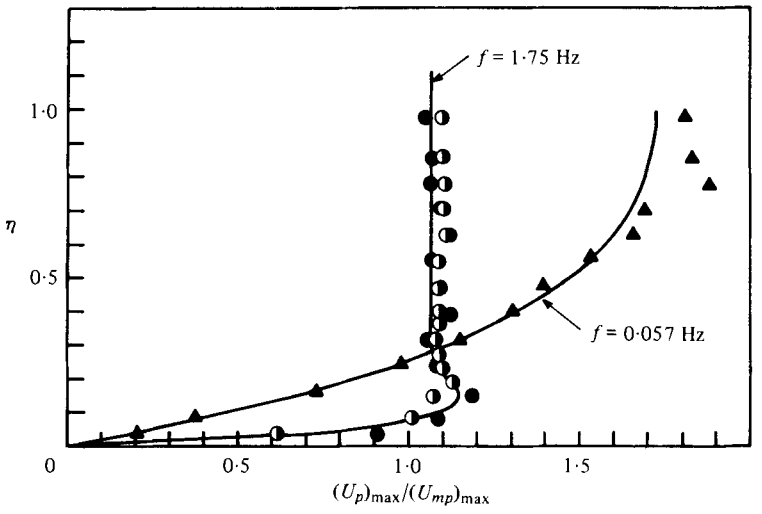

FIGURE 9. Distribution of the amplitude of the periodic component of velocity across the pipe. ● run 13 (f = 1·75 Hz); ◑, run 23 (f = 1·75 Hz); ▲, run 24 (f = 0·057 Hz); ——, laminar theory from Uchida (1956).

some important characteristic time scale of turbulence. In a wall-bounded flow, we can regard the turbulent burst frequency, f_t to determine such a characteristic time scale (at least near the wall). In the present case, the estimated burst frequency is about 2·3 Hz, (using the criterion $\bar{U}_m/f_t D \cong 5$ of Rao *et al.* 1971). The estimate is rough but is sufficient to indicate that one can expect to find interaction between the external oscillation and the internal turbulence structure when the flow pulsates at a frequency of 1·75 Hz. Stress-freezing is well documented in rapidly accelerated steady flows but studies of rapidly decelerated steady flows are difficult to perform, since the flow in such cases would separate very quickly. One of the interesting features of the present experiments is that the flow experiences large pressure gradients of alternating sign but yet does not actually separate. An estimate of the severity of the pressure gradient in the present case can be made by calculating the value of the Clauser pressure-gradient parameter β defined by (neglecting the shear effects),

$$\beta = \frac{D}{2\rho u_*^2}\frac{\partial P}{\partial x} \approx \frac{D}{2u_*}\frac{dU_m}{dt}. \tag{7}$$

Such a calculation shows that β varies from about -40 to about $+40$ during a cycle. The magnitudes of β attained during the cycle are comparable with the values for some of the severe adverse pressure gradient steady flows reported in the Proceedings of the Stanford Conference (Coles & Hirst 1968). Not only are the pressure gradients very large but they vary rapidly, the value of $d\beta/dt$ being of the order of 100 s^{-1} (based on a variation in β from 40 to -40 in half the period of oscillation). It is thus clear that the turbulent structure will be in a highly disturbed state. Hence, quasi-steady turbulence models based on local equilibrium assumption cannot be expected to describe the flow at such oscillation frequencies.

The quantity which is of greater value than u' in understanding the structure of turbulence is the Reynolds shear stress $-\rho\overline{uv}$. Unfortunately, on account of instrumentation limitations, it was not possible to make direct measurements of the

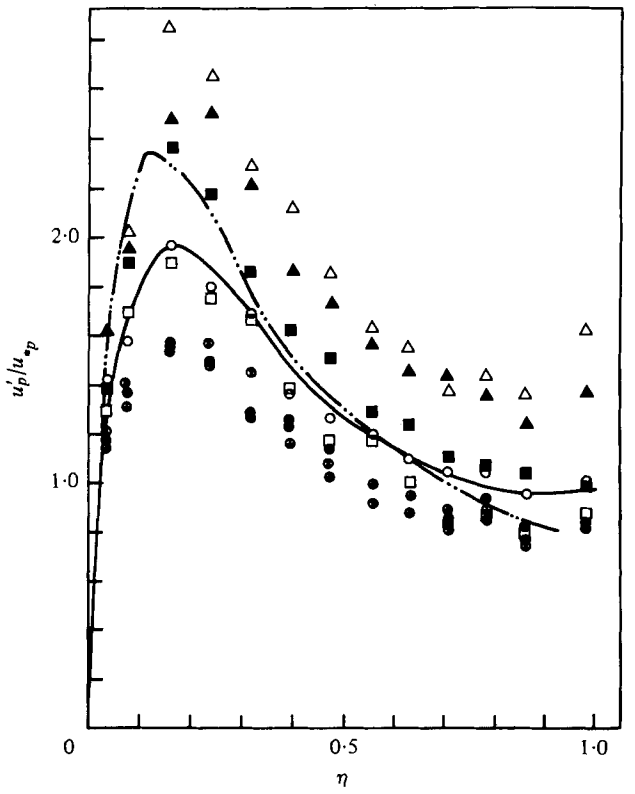

FIGURE 10. Distribution of the turbulent intensity across the pipe in run 13 (f = 1·75 Hz). ——, time-averaged turbulent intensity $u'/\bar{u}_*$ in oscillatory flow; – · · –, u'/u_* in quasi-steady flow at $\theta = 0°$. Data points denote the ensemble-average turbulent intensity u_p'/u_{*p} for the phase angles: ⊗, 6°, ⊕, 45°, ●, 90°; ○, 135°; ▲, 180°; △, 225°; ■, 270°; □, 315°.

Reynolds shear stress. However, it is possible to compute it, perhaps with some loss of accuracy, from the measured wall shear stress and velocity distribution. For this purpose, we write the instantaneous x-momentum equation for pipe flow as

$$\rho\frac{\partial U}{\partial t}+\rho U\frac{\partial U}{\partial x}+\rho V\frac{\partial U}{\partial r}=-\frac{\partial P}{\partial x}+\frac{1}{r}\frac{\partial(\tau r)}{\partial r} \tag{8}$$

where V is the instantaneous velocity in the radial direction. Performing an ensemble average on this equation, one gets, for fully developed unsteady turbulent flow,

$$\rho\frac{\partial\langle U\rangle}{\partial t}=-\frac{\partial\langle P\rangle}{\partial x}+\frac{1}{r}\frac{\partial\langle(\tau r)\rangle}{\partial r} \tag{9}$$

where

$$\langle\tau\rangle=\tau_{\text{laminar}}-\rho\langle uv\rangle. \tag{10}$$

We define $-\rho\langle uv\rangle$ as the ensemble-averaged Reynolds shear stress. Multiplying both sides of the equation (9) by $2\pi r$ and integrating across the pipe, and eliminating $\partial p/\partial x$, one gets (after inserting the phase average notations introduced earlier)

$$\frac{\tau}{\rho}(r,\theta)=\frac{1}{r}\int_0^r\frac{\partial}{\partial t}[\langle U(r,\theta)\rangle-U_m(\theta)]\,.\,r\,dr+\frac{2\tau_w(\theta)\,r}{D} \tag{11}$$

and

$$-\langle uv\rangle(r,\theta)=\frac{\tau}{\rho}(r,\theta)-\nu\frac{\partial\langle U(r,\theta)\rangle}{\partial r}. \tag{12}$$

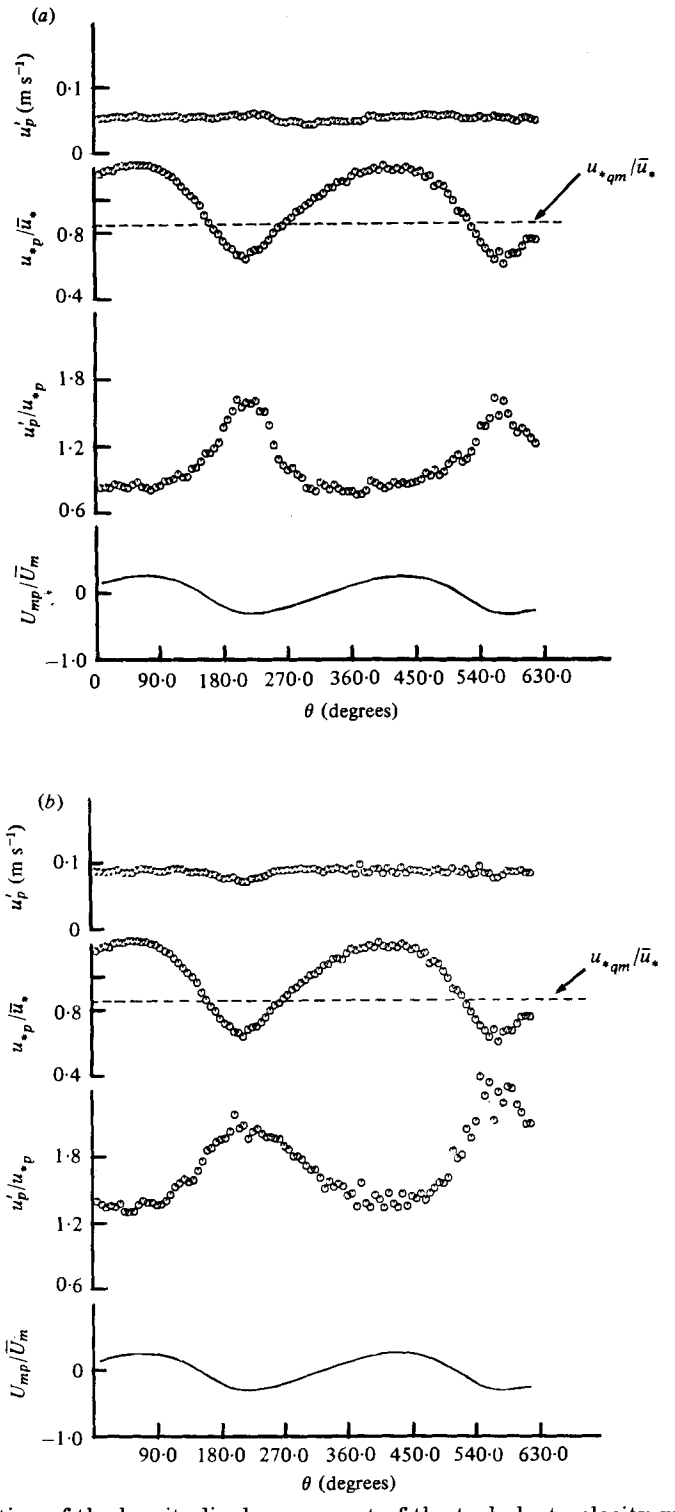

FIGURE 11. Variation of the longitudinal component of the turbulent velocity with phase angle in oscillatory flow at $f = 1{\cdot}75$ Hz. (*a*) $r = 0$; (*b*) $r = 23{\cdot}4$ mm (2 mm from the wall).

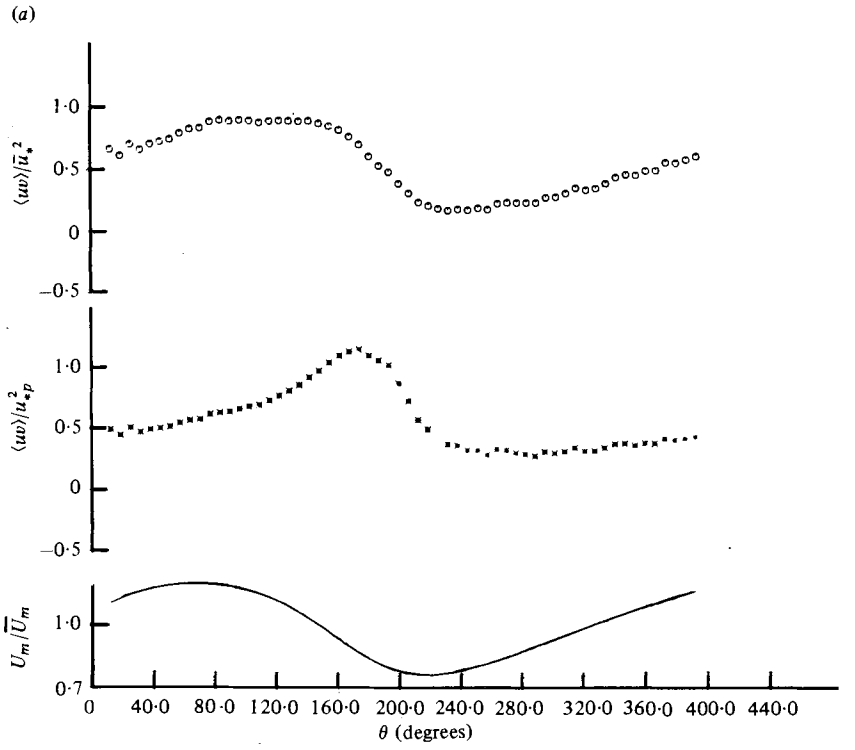

FIGURE 12. Variation of the Reynolds shear stress with phase angle in oscillatory flow, (*a*) 1 mm from the wall; (*b*) 2 m from the wall; (*c*) 10 mm from the wall.

The ensemble- (phase-) averaged Reynolds shear stress $-\langle uv\rangle$ was obtained from equations (11) and (12) using measured velocity and wall shear stress data. The process required differentiation with respect to time and integration across the pipe both of which were performed numerically on a computer. The velocity-time data were smoothed in order to reduce the numerical noise in differentiation. The procedure was found to work reasonably well because the velocity values were available at very close time intervals (50 values per cycle), velocity gradients in the radial direction were not severe (owing to the low Reynolds number of the flow), sufficient cycles were used for phase averaging (effectively 300) and lastly, the three terms in equation (12) were all of similar order of magnitude.

Variation of the ensemble averaged Reynolds shear stress during the cycle is shown in figures 12(*a*, *b*, *c*) for three typical locations in the pipe, viz. 1, 2 and 10 mm from the wall. Although there is some scatter in the data, the results are still good enough to allow one to arrive at meaningful conclusions especially in the region of flow where the Reynolds shear stress is significant. Very near the wall, $\langle uv\rangle$ shows a cyclical variation but lags behind U_m (and hence behind u_{*p} also). As the distance from the wall increases, the amplitude of variation of $\langle uv\rangle$ decreases until it becomes almost indistinguishable from scatter beyond the Stokes layer (as seen from figure 12*c*). The well-defined cyclical variation of $\langle uv\rangle$, in the inner layer (figures 12*a*, *b*) is in contrast to the frozen structure of u'_p. This suggests that the modulation in $\langle uv\rangle$ might have originated from modulations in the ensemble-averaged intensity, v'_p. This is possible

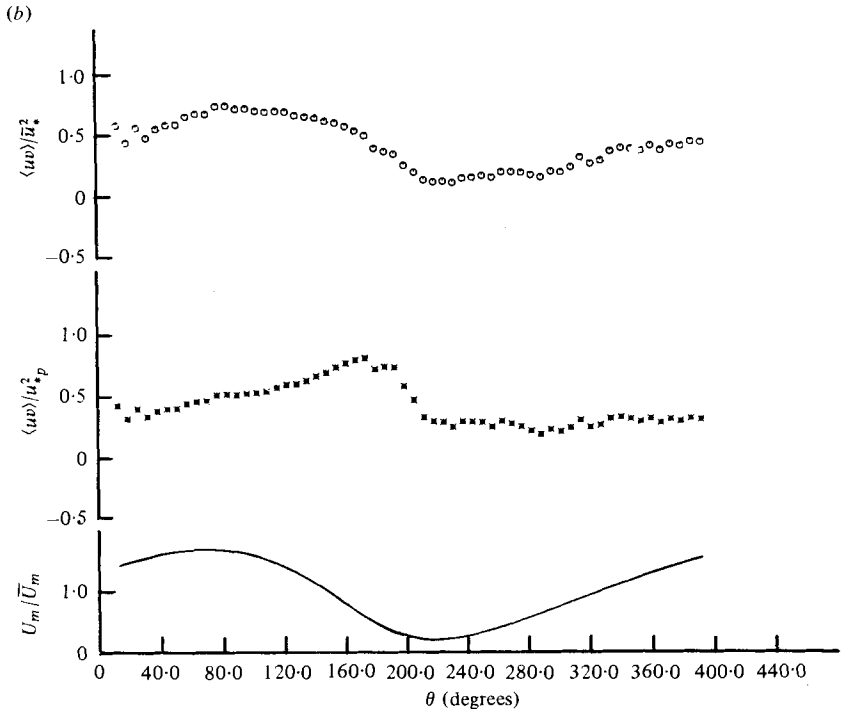

FIGURE 12(*b*). For legend see facing page.

since the v fluctuations are likely to be of finer scale than the u fluctuations (by a factor of nearly 5 as observed by Ramaprian 1975) and hence can respond more readily to the impressed oscillations. Since the time scale gets larger as the distance from the wall increases, the response of $\langle uv\rangle$ must be expected to diminish eventually in the core region. The nearly frozen structure of $\langle uv\rangle$ in the core region (figure 12*c*) thus indicates rapid strain rates. The departure from local equilibrium is again seen from the variations in $\langle uv\rangle/u_{*p}^2$ during the oscillation cycle.

Figure 13(*a*, *b*, *c*, *d*) are cross plots of the above data and show some typical distributions of the total, laminar and ensemble-averaged Reynolds shear stresses, across the pipe for fixed phase angles during the cycle. The distributions are normalized using the relevant inner-layer scales of velocity (u_{*p}) and length (ν/u_{*p}). The large variations in the distribution of the stresses from one point in the cycle to the other (seen more clearly from these figures) again indicate that the turbulence structure is far from equilibrium and hence cannot be described by quasi-steady models. Figure 14 shows the time-averaged distributions of each of the above stresses using $\bar{u}_*$ as the scaling velocity. These distributions were obtained by averaging the computed distributions at 50 phase positions in the cycle. It is seen that except for a slight discrepancy near the wall, the time-averaged total shear stress $\bar{\tau}$ shows the expected linear distribution. This indicates that there were no significant errors in the numerical procedure used for calculating the shear stresses from the experimental data. Some of the important features pertaining to figures 13 and 14 that require comments are the following.

(i) The laminar shear stress is significant up to a considerable distance from the

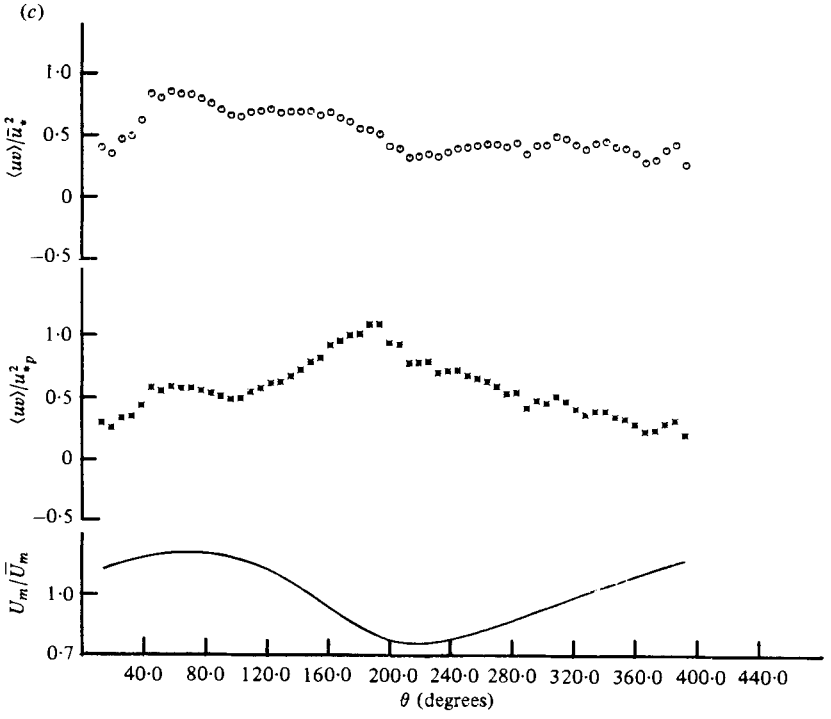

FIGURE 12(c). For legend see page 532.

wall. This is to be expected in view of the low Reynolds number of the flow.

(ii) The time-averaged turbulent shear stress reaches a maximum at about 6 mm ($\eta = 0{\cdot}25$) from the wall i.e., at about the same location where u' reaches a maximum. It is important to note that this is within the Stokes layer.

(iii) The time-averaged laminar shear stress distribution exhibits a local minimum near the wall. This is due to the presence of a point of inflexion in the time-mean velocity profile.

(iv) The distribution of the time-mean Reynolds shear stress also exhibits a kink within the Stokes layer. Also, it is observed that, in the region very close to the wall, the time-mean Reynolds shear stress attains a value larger than in steady flow.

(v) The time-mean distributions of the stresses are not significantly different from the corresponding distributions in steady flow, in the region beyond the Stokes layer. However, by affecting the distributions within the Stokes layer, the imposed unsteadiness produces an increase in the time-mean velocity gradient at the wall and hence increases the wall shear stress. This is seen from figures 11(*a*, *b*), where the quasi-steady mean value, u_{*qm} (obtained from pressure drop measurements), is shown as a horizontal dashed line against the distribution of u_{*p} in unsteady flow. The time-mean value of u_{*p} is clearly larger than the quasi-steady mean value of u_*.

The quantity, $E_p = \int_0^R \left\{\langle\tau\rangle \frac{\partial\langle U\rangle}{\partial r}\right\} 2\pi r\, dr$, represents the rate of work done per unit length of pipe by the shear stress and hence its average value over an oscillation cycle represents the power loss in the pipe. The term E_p normalized with respect to

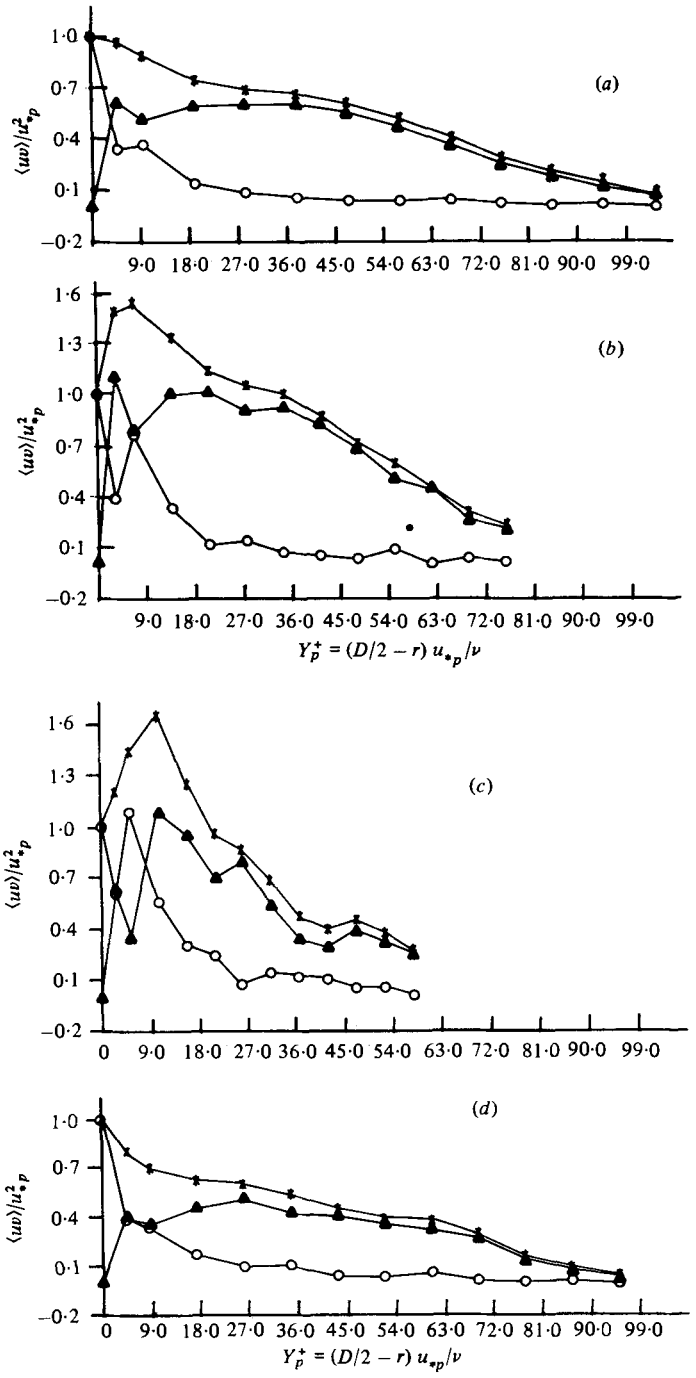

FIGURE 13. Distribution of total, laminar and Reynolds shear stresses across the pipe in wall-layer co-ordinates at prescribed phase angles. (*a*) $\theta = 77°$, (*b*) $\theta = 160°$, (*c*) $\theta = 212°$, (*d*) $\theta = 340°$. —*—, total shear stress; —○—, laminar shear stress; —▲—, Reynolds shear stress. The stresses are normalized with respect to the wall shear stress at the corresponding phase angle.

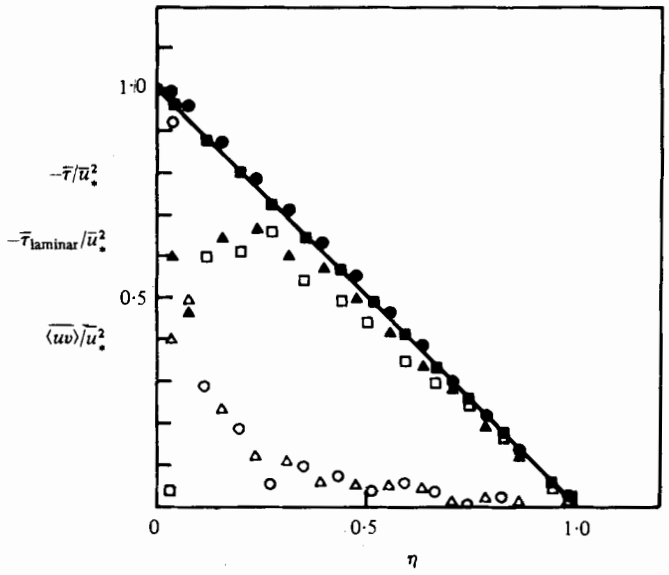

FIGURE 14. Distribution of the time-averaged total, laminar and Reynolds shear stresses across the pipe. Steady turbulent flow at a Reynolds number of 2870 ($\theta = 0°$): ■, total shear stress; □, Reynolds shear stress; ○, laminar shear stress. Unsteady turbulent flow, $f = 1{\cdot}75$ Hz (run 13): ●, total shear stress; ▲, Reynolds shear stress; △, laminar shear stress.

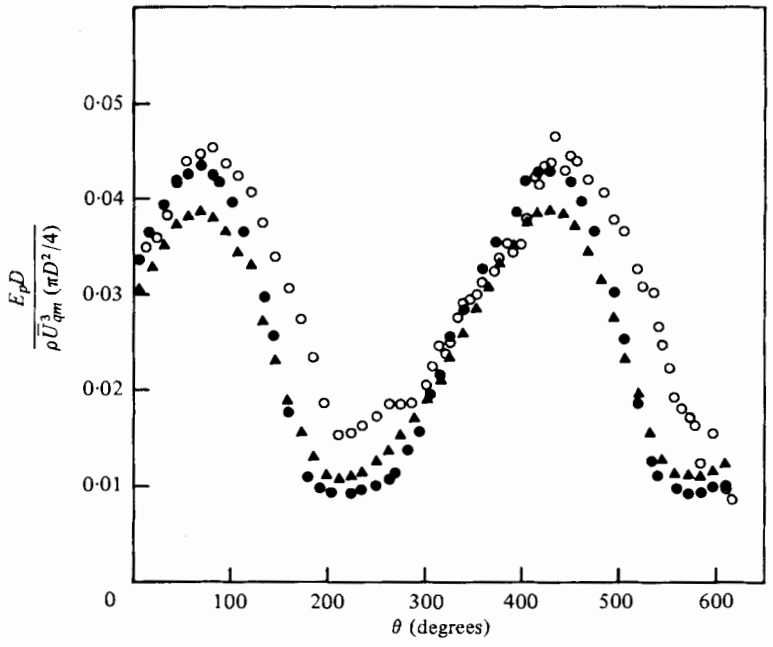

FIGURE 15. Variation of the rate of shear work with the phase angle. ○, data from unsteady turbulent flow, $f = 1{\cdot}75$ Hz (run 13); ▲, based on quasi-steady Blasius relation, $\lambda = 0{\cdot}3165\, Re^{-\frac{1}{4}}$; ●, based on quasi-steady pressure drop measurements in actual transitional flow.

($\rho \bar{U}_{qm}^3 \pi D/4$) is shown in figure 15 as a function of the phase angle. The corresponding power loss in a hypothetical quasi-steady turbulent flow can be obtained for the same Reynolds number modulation using the Blasius relation, $\lambda = 0{\cdot}3165\, Re^{-\frac{1}{4}}$. Also, for the *actual transitional* quasi-steady flow, the power loss for the same Reynolds number can be obtained from the measured quasi-steady pressure drop. Both these distributions are also shown in figure 15. It is seen that flow oscillation in run 13 at a high frequency results in an increase in average power loss when compared with the quasi-steady *transitional* flow. This is, however, to be expected since the unsteady flow is fully turbulent during the entire cycle, whereas the quasi-steady flow is not. However, it is significant to note that the unsteady flow has a slightly higher average power loss when compared to the hypothetical *fully turbulent* quasi-steady flow also.

(*b*) *Results of series* 2 *experiments*: (*laminarized unsteady flow*). During the second series of experiments, the unsteady flow remained nearly laminar. Since this was a very significant observation, it was carefully verified to insure that the laminarization was not due to any obvious reasons such as an increase in fluid viscosity, reduction in flow velocity, etc. Starting from a fully turbulent flow at the fully open slot position, the flow could be laminarized by just rotating the sleeve at the lowest possible speed (0·047 Hz).

A careful study of the oscilloscope traces of the velocity signal at several oscillation frequencies indicated, however, that laminarization was not always complete, and that the oscillatory flow did, in fact, become turbulent at times. The intermittency of this occurrence depended on the oscillation frequency. In order to make a more detailed study of this phenomenon, several long-time records of the LDA signal were obtained using a strip chart recorder. The record length in all the cases was equal to 300 cycles or 5 minutes whichever was longer. Records were obtained for $r = 0$ and $r = 18{\cdot}4$ mm. Similar records were obtained in quasi-steady flow also for comparison. A few typical records are shown in figures 16 and 17. It is seen that the flow does become turbulent several times during the duration of the record. Estimating the intermittency of turbulence from such records is no doubt difficult and subjective; particularly when turbulent and oscillation frequencies are not well separated. The following procedure was arbitrarily selected for making a rough estimate of the intermittency. The procedure is based on the observation (and assumption) that whenever the flow became turbulent, its velocity level would jump upwards or downward from the laminar value depending on whether the point under consideration was in the wall region or on the centre-line. In both the cases, a distortion would be observed in the velocity signal recorded on the strip chart. The dynamic response of the recorder (5 Hz) was adequate for indicating this distortion. A short length of the laminar record traced out on a transparent sheet would be moved over the record and portions of the record that did not coincide with the laminar record would be marked out as turbulent intervals. The intervals marked T in figure 17 correspond to typical turbulent intervals. The intermittency factor, γ was defined as the ratio of the turbulent interval to the total record length. In the case of steady flow, the turbulent intervals could be easily recognized without much ambiguity.

The intermittency factor is plotted in figure 18 for quasi-steady flow as a function of quasi-steady Reynolds number. It is seen that the mean quasi-steady flow ($\theta = 90°$, i.e. $Re \simeq 2100$) has an intermittency of about 0·2. The intermittency factor for oscillatory flow is shown in figure 19 as a function of oscillation frequency. A parameter

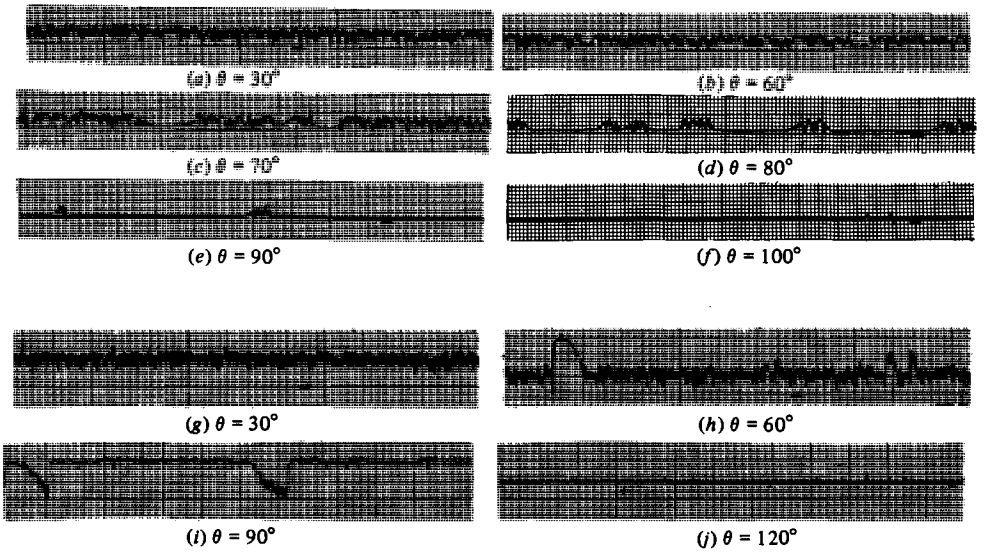

FIGURE 16. Typical strip chart records of the LDA output signal in steady flow from experimental series 2. (*a*)–(*f*) r = 18·4 mm. (*g*)–(*j*) r = 0.

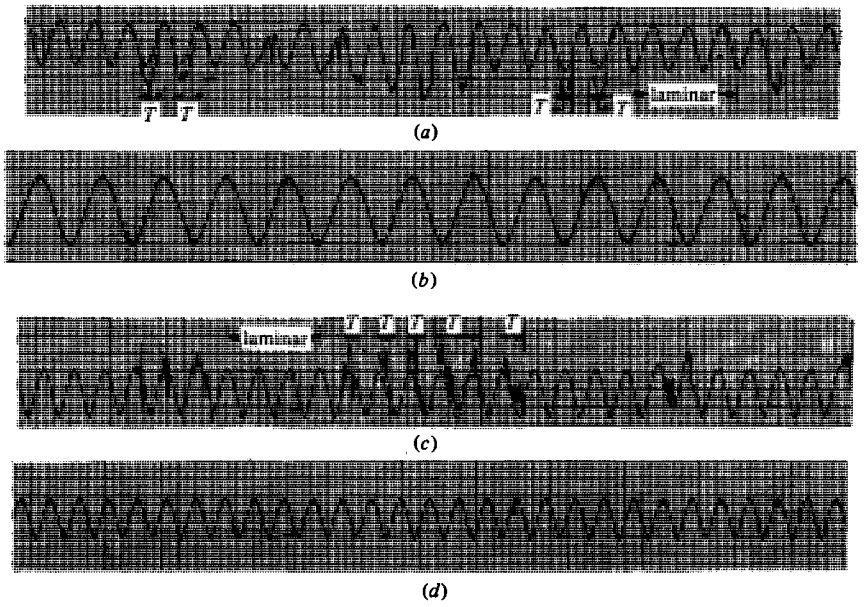

FIGURE 17. Typical strip chart records of the LDA output signal in oscillatory flow from experiment series 2. For r = 0, (*a*) f = 0·23 Hz, (*b*) f = 0·057 Hz. For r = 18·4 mm, (*c*) f = 0·23 Hz, (*d*) f = 0·057 Hz. Intervals marked T denote periods when the velocity trace is distorted from the normal laminar shape (shown by dotted lines) and are hence assumed to represent durations of turbulent puffs. (Not all turbulent intervals are marked.)

often used in characterizing laminar oscillatory pipe flows is the Stokes number Ω defined as $[D/2(2\pi f/\nu)^{\frac{1}{2}}]$. It is seen that Ω is proportional to the ratio of the pipe radius to the thickness of the Stokes layer. The values of Ω are also shown in figure 19. The data for unsteady transitional flow show some interesting trends. The intermittency is very low at either end of the frequency range studied (Ω = 4–22). However, it increases fairly significantly and appears to reach a maximum around an oscillation frequency of about 0·4 Hz ($\Omega \cong 12$). This maximum intermittency factor attained, is not very small and, at r = 18·4 mm, is indeed comparable to that of the mean quasi-steady flow. Lastly, the data indicate different values for intermittency near the wall and at the centre. It is interesting to note that Yellin (1966) also observed that when transition occurred in pulsatile flows, the disturbances were typically restricted to the core. However, the authors have no explanation at this time for this behaviour of the flow. The other aspects of transition in oscillatory flows are examined in some detail below.

Wygnanski & Champagne (1973) have reported detailed study of the steady transitional pipe flow. They divide intermittent transitional turbulence into two categories – the 'puff' type and the 'slug' type. Puffs are caused by large disturbances at the inlet region of the pipe and are actually remnants of a partial relaminarization process. Slugs, on the other hand, originate from the instability of the boundary layer and represent various stages of amplification of these disturbances. The puffs usually occur in the Reynolds number range of 2000–2700 while the slugs appear generally at very much larger Reynolds numbers. The intermittency measurements in steady flow in the present case are compared in figure 18 with the puff flow data from Wygnanski & Champagne. The qualitative agreement between the two sets of data suggests that the present transitional flow can be regarded as a 'puff'-type flow. This is further borne out by the fact that the turbulent puffs are of approximately the same intensity near the wall as at the centre-line (as seen from the strip chart record), unlike a slug-type flow which is known to exhibit an increase in intensity from the centre-line to the wall. It may be noted also that the flow is fully turbulent at about Re = 2700.

The development of turbulence through a puff-type transition process does not depend on shear layer instability near the pipe wall since the disturbance is provided by the inlet conditions but depends on the existence of a Reynolds number above a critical value so that the initial turbulence can be sustained. This threshold critical value is about 2000 and transition to turbulence can not occur below this Reynolds number.

In a flow subjected to a favourable pressure gradient, this critical Reynolds number is known to increase. But, in an adverse pressure gradient, it will *not* decrease significantly below the threshold value. Hence, if the Reynolds number of flow oscillates around 2000, the net effect would be an increase in the critical Reynolds number and hence a partial or complete laminarization of the initial turbulent puffs. The increase in the critical Reynolds number will be larger at larger favourable pressure gradients and hence one would expect to find a greater degree of laminarization as the oscillation frequency increases. This is, exactly what is observed in figure 19 as a decrease in the intermittency in the range of 0·4 Hz–1·75 Hz (Ω = 12–22) with the flow being almost completely laminar at 1·75 Hz. The existence of a maximum intermittency (almost equal to the intermittency in the mean steady flow) at about 0·4 Hz

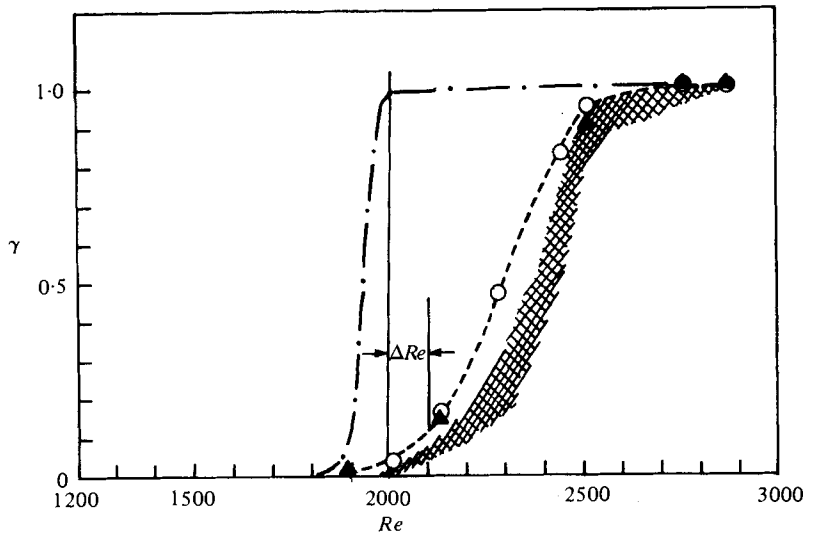

FIGURE 18. The intermittency of turbulent puffs in steady flow. Data from present series 2 experiments: – –▲– –, $r = 0$; – –○– –, $r = 18{\cdot}4$ mm. – · –, (estimated) intermittency data for steady flow experiments of series 1; ▨. data of Wygnanski & Champagne (1973).

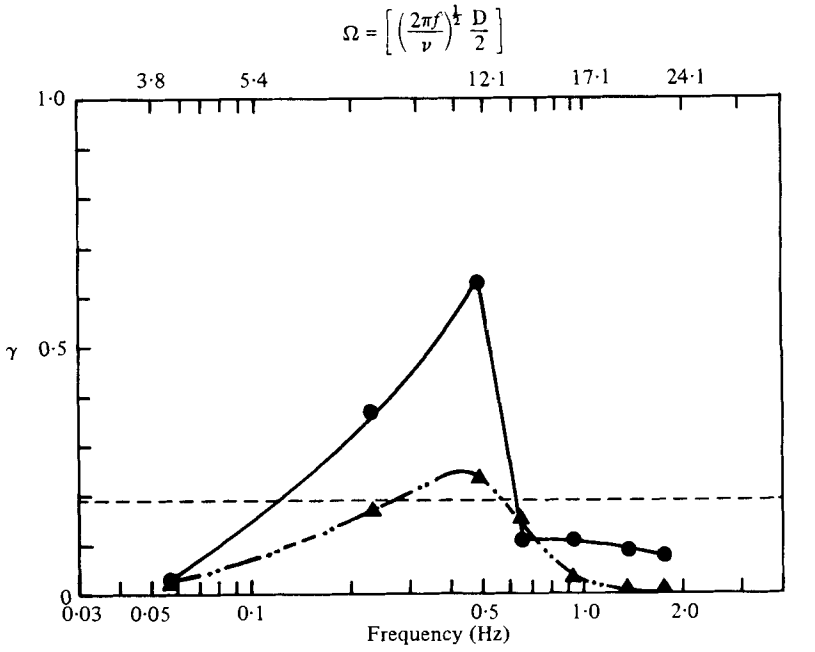

FIGURE 19. The intermittency of turbulent puffs in oscillatory flow from experiment series 2. —●—, $r = 0$ mm; ···▲···, $r = 18{\cdot}4$ mm; – – – –, mean quasi-steady flow at $Re = 2100$ ($\theta = 90°$).

($\Omega \cong 12$) appears somewhat to contradict the above argument. It is, however, important to note that at low frequencies, (0 – 0·4 Hz), ($\Omega = 0$–12) the favourable pressure gradients are very small (at the amplitude of modulation employed) and consequently, the effect on the critical Reynolds number is negligibly small at these frequencies. On the other hand, the extent of laminarization of the puffs depends not only on the critical Reynolds number but also on the length of time in a cycle the puffs are exposed to a Reynolds number lower than the critical Reynolds number. At low frequencies the latter effect becomes dominant and since the residence time of the puffs below the critical Reynolds number increases as the oscillation frequency is reduced, the intermittency of puffs would decrease with frequency in this range. The results in this range agree qualitatively with those of Sarpkaya (1966) whose experiments extended over the range $\Omega = 4$–7·8. He found that at small amplitudes of modulation ($\lambda = 0{\cdot}2$–0·3) there was only a slight increase in critical Reynolds number above the steady state value and that increase in the oscillation frequency in this range reduced the rise in critical Reynolds number. Sarpkaya noticed negligible effect of oscillation in the transition characteristics at $\Omega = 7{\cdot}8$ (which, incidentally, he regarded as 'rapid' oscillation). It is interesting to note that at about 0·4 Hz corresponding to $\Omega \cong 12$ the present unsteady flow exhibits the maximum intermittency. The present observations are thus in qualitative agreement with those of Sarpkaya. There is, however, quantitative disagreement between the present data and those of Sarpkaya with respect to the actual magnitudes of the critical Reynolds number at the various values of Ω. This is due largely to the difference between the definitions of critical Reynolds number used in the two cases. In the present case, the critical Reynolds number is taken to be the Reynolds number at which the puffs (external disturbances) disappear whereas Sarpkaya defined it as the Reynolds number at which the external disturbances cease to amplify. It is thus clear that the present definition describes the lower bound for the puff-type transition process.

The major difficulty with studies connected with puff-type transition is that the process is very sensitive to the nature of external disturbances and other ambient conditions. It is thus very difficult to find repeatability in observations over a period of time. This is especially true when an additional factor, namely flow oscillation, is introduced. This has been clearly demonstrated by the two series of experiments reported in this paper. The two series gave entirely different results under what apparently appeared to be identical conditions. It is worth examining the reasons for this at least in a qualitative way. As mentioned already, the mean steady flow ($\theta = 90°$) was fully turbulent in the series 1 experiments. In fact, it was fully turbulent even at $\theta = 100°$ (corresponding to $Re \cong 2000$). Unfortunately, intermittency measurements were not made in these series. However, one can visualize (without much error) the intermittency variation with Reynolds number to be as shown in figure 18. It is very clear that in this flow, transition occurred within a very narrow range of Reynolds numbers, unlike in the second series of experiments in which it was spread over a much wider range of Reynolds numbers. The reason for this difference in behaviour between the two flows is not known. However, the two intermittency distributions shown in figure 18 for the two series can be used to explain qualitatively the observed difference in response of the flow to oscillation at a high frequency in the two cases. Flow oscillation at a high frequency would raise the critical Reynolds number from its value of about 2000 at quasi-steady state by an amount, say, ΔRe. This is equivalent

to moving the operating line, i.e. mean flow Reynolds number of the unsteady flow to the left by ΔRe in figure 18. It is seen that in the series 2 experiments, the new operating line corresponds to a laminarized flow (of very small intermittency) while in the series 1 experiments, it corresponds to fully turbulent flow (of intermittency 1). It is to be mentioned here that laminarized oscillatory flow can be observed only under very restricted conditions. These include puff-type transition (i.e., transition brought about by inlet disturbances), a relatively small intermittency of puffs at the mean Reynolds number and either strong pressure gradient fluctuations (high frequency, large amplitude oscillation), or large puff-residence time (long enough pipe). These conditions are often found in the pulsatile flow of blood in the mammalian aorta and hence laminarization of the flow can be expected to occur in such cases. This is, in fact, corroborated by some of the recent *in-vivo* aorta experiments mentioned at the beginning of this paper.

4. Conclusions

The present study has led to the following conclusions.

(i) Periodic oscillation of discharge tends to increase the critical Reynolds number of puff-type transitional pipe flow. Under certain conditions, the transitional flow may be laminarized on periodic oscillation. For a given amplitude of flow modulation the extent of laminarization depends on factors such as the intermittency of puffs in the quasi-steady mean flow, the oscillation frequency and the residence time of the puffs in the pipe.

(ii) The laminarized periodic flow behaves very much like laminar periodic flow. For example, the time-mean flow properties remain unchanged from those of quasi-steady mean flow and the phase lag and amplitude of the periodic velocity component depend strongly on the Strouhal number.

(iii) When the oscillatory flow is fully turbulent, its periodic structure still qualitatively resembles that of oscillatory laminar flow at the same Strouhal number. However, the behaviour of the oscillatory turbulent flow is also influenced by an additional parameter, namely the ratio of the oscillation frequency to some characteristic frequency of turbulence. When this ratio is of the order unity, the oscillations interact with the turbulent structure. Important quantitative differences can be observed between laminar and turbulent flows at such interactive oscillatory frequencies. For example, the time-mean velocity profile in the oscillatory flow exhibits a point of inflexion near the wall, and the time-mean wall shear stress and power loss increase from their quasi-steady values. Also, the periodic velocity component exhibits an overshoot in the Stokes layer, the magnitude of the overshoot being larger than in laminar oscillatory flows at the same Strouhal number.

(iv) At the interactive frequency of oscillation, mentioned above, the ensemble-averaged turbulence intensity is frozen everywhere in the pipe. The ensemble averaged Reynolds shear stress is able to follow the oscillation cycle (with some lag) only very close to the wall. However, beyond the Stokes layer, it is also frozen at some averaged value. The stress freezing is brought about by the large and rapidly varying strain rates. The ensemble-averaged Reynolds stress does not scale with the corresponding ensemble-averaged wall shear stress indicating significant departures from local structural equilibrium.

As mentioned at the very beginning, the previous experiments on periodic turbulent flows have generally led to the conclusion that impressed flow oscillation has no effect on the time-mean properties of the flow. Predictions based on some quasi-steady turbulence models have also supported this conclusion. The observed effect of flow oscillation on the time-mean flow in the present experiments is thus a new and significant result. While it is consistent with the presence of rapid strain rates associated with the high oscillation frequency of the flow and the attendant stress freezing phenomenon, it is, nevertheless, important to perform more experiments (preferably at much higher Reynolds numbers) to corroborate this result.

The authors gratefully acknowledge the support received from the Biomedical Grants Research Program of the Graduate College of The University of Iowa and the United States Army Research Office Grant no. DAAG-79-G-0017.

REFERENCES

ACHARYA, M. & REYNOLDS, W. C. 1975 Measurements and predictions of a fully developed turbulent channel flow with imposed controlled oscillations. *Stanford Univ. Thermosciences Div., Tech. Rep.* no. TF-8.

COLES, D. A. & HIRST, E. A. 1968 *Proc.* 1968 *Stanford Conf. on Boundary Layers.*

COUSTEIX, J., DESOPPER, A. & HOUDEVILLE, R. 1977 Structure and development of a turbulent boundary layer in an oscillatory external flow. *Proc. Symp. on Turbulent Shear Flows, Penn. State Univ., Univ. Park, Pa.*

FALSETTI, H. L., KISER, K. M., FRANCIS, G. P. & BELMORE, E. R. 1972 Sequential velocity development in the ascending aorta of the dog. *Circulation Res.* **31**, 328–338.

GERRARD, J. H. 1971 An experimental investigation of the pulsating turbulent water flow in a tube. *J. Fluid Mech.* **46**, 43–64.

HINO, M. & SAWAMOTO, M. 1975 Linear stability analysis of an oscillatory flow between parallel plates. *Proc. 7th Symp. on Turbulence* (ed. H. Sato & M. Ohji), pp. 1–7. Inst. of Space & Aeronautics, Univ. of Tokyo.

HINO, M., SAWAMOTO, M. & TAKASU, S. 1976 Experiments on transition to turbulence in an oscillatory pipe flow. *J. Fluid Mech.* **75**, 193–207.

HIROSE, K. & OKA, T. 1969 The friction factors of unsteady pipe flows. *Mem. Sch. Engng, Okayama Univ.* **4**, 9–12.

HOUDEVILLE, R., DESOPPER, A. & COUSTEIX, J. 1976 Experimental analysis of average and turbulent characteristics of an oscillatory boundary layer. *Pro. Euromech* 73, *Aix-en-Provence.*

HOUDEVILLE, R. & COUSTEIX, J. 1978 Premiers Resultats d'une etude sur les couches limites turbulentes en ecoulement pulse avec gradient de pression moyen defavourable. 15*e Coll. D'Aerodynamique Appl., Marseille.*

KARLSSON, S. K. F. 1959 An unsteady turbulent boundary layer. *J. Fluid Mech.* **5**, 622–636.

KENISON, R. C. 1977 An experimental study of the effect of oscillatory flow on separation region in a turbulent boundary layer. *AGARD Symp. on Unsteady Aerodynamics, Ottawa.*

KERCZEK, C. VON & DAVIS, S. H. 1974 Linear stability theory of oscillatory Stokes layers. *J. Fluid Mech.* **62**, 753–773.

KERCZEK, C. VON & DAVIS, S. H. 1976 The instability of a stratified periodic boundary layer. *J. Fluid Mech.* **75**, 287–303.

KISER, K. M., FALSETTI, H. L., YU, K. H., RESITARITS, M. R., FRANCIS, G. P. & CARROLL, R. J. 1976 Measurements of velocity wave forms in the dog aorta. *Trans. A.S.M.E.* I, *J. Fluids Engng* **6**, 297–304.

LAUFER, J. 1954 The structure of turbulence in fully developed pipe flow. *NACA Rep.* 1174.

LU, S. Z., NUNGE, R. J., ERIAN, F. F. & MOHAJERY, M. 1973 Measurements of pulsating turbu-

lent water flow in a tube. *Prog. 3rd Symp. on Turbulence in Liquids, Univ. of Missouri, Rolla*, pp. 375–392.

PATEL, M. H. 1977 On turbulent boundary layers in oscillatory flow. *Proc. Roy. Soc.* A **353**, 121–144.

RAMAPRIAN, B. R. 1975 Turbulence measurements in an 'equilibrium' axisymmetric wall jet. *J. Fluid Mech.* **71**, 317–338.

RAMAPRIAN, B. R. & TU, S. W. 1979 Experiments on transitional oscillatory pipe flow. *Inst. Hydraulic Res., Univ. Iowa. IIHR Rep.* no. 221.

RAO, K. N., NARASIMHA, R. & BADRI NARAYANAN, M. A. 1971 The 'bursting' phenomena in a turbulent boundary layer. *J. Fluid Mech.* **48**, 339–352.

RICHARDSON, E. G. & TYLER, E. 1929 The transverse velocity gradient near the mouthes of pipes in which an alternating or continuous flow of air is established. *Proc. Phys. Soc. Lond.* **42**, 1–15.

ROSENHEAD, L. 1963 *Laminar Boundary Layers*. Oxford University Press.

SARPKAYA, T. 1966 Experimental determination of the critical Reynolds number for pulsating Poiseuille flow. *Trans. A.S.M.E.* D, *J. Basic Engng* **88**, 589–598.

SCHULTZ-GRUNOW, F. 1940 *Pulsierender Durchfluss durch Rohre*. Porschung **11**, 170–187. (Pulsation flow through pipes. *N.A.S.A. Technical Transl.* NASA-TT-F-14881, 1973.)

TU, S. W. 1978 An experimental study of oscillatory pipe flow at transitional Reynolds numbers. M.S. thesis, Mechanics and Hydraulics Program, The University of Iowa.

UCHIDA, S. 1956 The pulsating viscous flow superposed on the steady motion of incompressible fluid in a circular pipe. *Z. angew. Math. Phys.* **7**, 403–421.

WYGNANSKI, I. J. & CHAMPAGNE, F. H. 1973 On transition in a pipe. Part I. The origin of puffs and slugs and the flow in a turbulent slug. *J. Fluid Mech.* **59**, 281–336.

YELLIN, E. L. 1966 Laminar turbulent transition process in pulsatile flow. *Circ. Res.* **19**, 791–804.